

Fully analytical equation of motion approach for the double quantum dot in the Coulomb blockade regime

Nahual Sobrino,^{1,*} David Jacob,^{1,2} and Stefan Kurth^{1,2,3}

¹*Nano-Bio Spectroscopy Group and European Theoretical Spectroscopy Facility (ETSF),
Departamento de Polímeros y Materiales Avanzados: Física,
Química y Tecnología, Universidad del País Vasco UPV/EHU,
Avenida de Tolosa 72, E-20018 San Sebastián, Spain*

²*IKERBASQUE, Basque Foundation for Science, Plaza Euskadi 5, E-48009 Bilbao, Spain*

³*Donostia International Physics Center (DIPC),
Paseo Manuel de Lardizabal 4, E-20018 San Sebastián, Spain*

(Dated: September 13, 2024)

A fully analytical approach based on the equation of motion technique to investigate the spectral properties and orbital occupations in an interacting double quantum dot in equilibrium is presented. By solving a linear system for the density correlators analytically, an explicit expression for the one body Green's function in terms of local occupations, intra- and inter-dot Coulomb interactions, and the model parameters is derived. In the uncontacted limit, the results coincide with those obtained from the grand canonical ensemble. The analytical results compare favorably with numerical results obtained with the non-crossing approximation and the hierarchical equation of motion methods accurately reproducing peak positions and spectral weight distributions in the Coulomb blockade regime.

I. INTRODUCTION

In the last decades quantum dots (QDs) have attracted an enormous amount of attention due to their potential applications in quantum computing, nanoelectronics, and as ideal systems to explore fundamental quantum phenomena[1–9]. QDs are essentially nanostructures that confine electrons within a small region of space, leading to the quantization of the electronic motion in all dimensions. They can be realized in manifold ways, e.g., by electrostatic confinement of a two-dimensional electron gas [1], metallic or semiconductor nanoparticles [10, 11], carbon nanotubes [12, 13], or the buckminster fullerene (C₆₀) [14].

A QD coupled to electrodes can be effectively described by an Anderson impurity model (AIM)[15], which has been a cornerstone for understanding strongly correlated electronic systems. The AIM offers an ideal playground to explore electron-electron interactions, shedding light on phenomena such as the Kondo effect and magnetic impurity behavior in metals, significantly advancing our understanding of many-body physics[16]. These insights have paved the way for exploring more complex systems, such as double quantum dots (DQDs), which offer a unique platform for investigating electron-electron interactions, quantum coherence, and transport properties in low-dimensional systems. The coupling between QDs and the presence of interdot interactions introduce complex and intriguing physics that have been extensively studied in and out of equilibrium both theoretically and experimentally [17–24].

Various computational approaches have been devel-

oped for solving the AIM and its extensions, among them numerical renormalization group (NRG), quantum Monte Carlo (QMC), non-crossing approximation (NCA), and hierarchical equations of motion (HEOM)[25–33]. On the other hand, the equation of motion (EOM) approach has emerged as a powerful tool for investigating Green's functions in Hubbard and Anderson impurity models[34–38]. The EOM approach provides a systematic way to derive the equations governing the dynamics of the Green's functions (GFs), allowing for a detailed analysis of the spectral properties and electronic correlations. This approach has been successfully applied to study the spectral and transport properties of single and multiple quantum dot systems under various interaction regimes[39–51]. However, the complexity of the equations due to inter-dot interactions and coupling to electronic reservoirs required different approximations and numerical techniques to accurately describe correlated electronic states and transport phenomena.

Despite the progress made using numerical techniques, an analytical approach offers the distinct advantage of providing explicit functional dependencies. Understanding these dependencies is crucial for designing and optimizing quantum dot-based devices, particularly in regimes where strong electron-electron interactions play a dominant role. Furthermore, analytical solutions offer a computationally efficient way to study additional properties and explore new physical regimes, guiding experimental efforts and advancing the development of quantum technologies.

The rest of the paper is organized as follows: In Sec. II, we first introduce the DQD Hamiltonian coupled to reservoirs, and explain in detail our analytic solution for the DQD via the EOM approach. In Sec. III, we provide a comprehensive comparison of the analytical results with numerical methods, discussing the accuracy and reliabil-

* nahualcarlos.sobrinoc@ehu.eus

ity of the analytical EOM approach. The conclusions are presented in Sec. IV. Finally, we provide details of the derivations in three Appendixes: Appendix A details our approximate treatment of the leads, Appendix B gives details for the different GFs while Appendix C presents the linear system for the density correlators and its analytical solution.

II. MODEL AND METHOD

A. Double quantum dot model

We consider a parallel double quantum dot (DQD) system, where each quantum dot (QD) $i = 1, 2$ is attached to its own left (L) and right (R) reservoirs of non-interacting electrons. The Hamiltonian of the system has the form

$$\begin{aligned} \hat{\mathcal{H}} = & \sum_i v_i \hat{n}_i + \sum_i U_i \hat{n}_{i\sigma} \hat{n}_{i\bar{\sigma}} + U_{12} \hat{n}_1 \hat{n}_2 \\ & + \sum_{\alpha k \sigma} \epsilon_{\alpha k i} \hat{c}_{\alpha k i \sigma}^\dagger \hat{c}_{\alpha k i \sigma} + \sum_{i \alpha k \sigma} \left(V_{\alpha k i} \hat{c}_{\alpha k i \sigma}^\dagger \hat{d}_{i\sigma} + \text{H.c.} \right), \end{aligned} \quad (1)$$

where $\hat{d}_{i\sigma}$ ($\hat{d}_{i\sigma}^\dagger$) is the annihilation (creation) operator for an electron with spin σ on QD i , and $\hat{c}_{\alpha k i \sigma}$ ($\hat{c}_{\alpha k i \sigma}^\dagger$) is the annihilation (creation) operator for an electron in state k, σ in reservoir $\alpha = \text{L, R}$ connected to dot i . $\hat{n}_i = \sum_\sigma \hat{n}_{i\sigma}$ and $\hat{n}_{i\sigma} = \hat{d}_{i\sigma}^\dagger \hat{d}_{i\sigma}$ are the total and the spin resolved occupation operators for QD i , respectively.

The first three terms in Eq. (1) describe the DQD with on-site energies (or gates) v_i and subject to intra- and inter-dot Coulomb repulsion U_i and U_{12} , respectively. The last two terms in Eq. (1) describe the single-particle eigenstates of the reservoirs with energies $\epsilon_{\alpha k i}$ and the coupling to the corresponding QD with hopping $V_{\alpha k i}$.

B. Analytical equation of motion approach

We now apply the EOM approach to obtain an analytic expression for the single-particle GF solely in terms of the occupations $\langle \hat{n}_i \rangle$ of each QD i and the electron addition and removal energies. The derived expression is valid for the weak-coupling regime, i.e. when the coupling to the reservoirs is small compared to the temperature, and becomes exact in the limit of vanishing coupling, in contrast to other approaches, which usually rely on some kind of mean-field decoupling [45, 46]. Our approach consists of two steps: First the EOMs are solved recursively, leading to expressions for both the single-particle as well as higher-order GFs in terms of density correlators $\langle \hat{n}_{i_1 \sigma_1} \hat{n}_{i_2 \sigma_2} \dots \rangle$ where the brackets $\langle \dots \rangle$ indicate the thermal average, i.e., $\langle \hat{A} \rangle = \text{Tr}[e^{-\beta \hat{\mathcal{H}}} \hat{A}] / \text{Tr}[e^{-\beta \hat{\mathcal{H}}}]$ with the inverse temperature $\beta \equiv 1/T$. From the equations for the GFs, in a second step we obtain a set of linear

equations for the correlators, which in the case of the DQD can be solved analytically. The solution allows us to express the correlators and thus the GF in terms of the dot occupations $\langle \hat{n}_i \rangle$.

The retarded single-particle GF of the DQD system given in Eq. (1) is defined in the time domain as

$$G_{i\sigma}^r(t) = -i\theta(t) \langle \{ \hat{d}_{i\sigma}(t), \hat{d}_{i\sigma}^\dagger(0) \} \rangle, \quad (2)$$

where $\theta(t)$ is the Heaviside step function, the curly brackets denote the anticommutator, and for any operator \hat{A} the corresponding operator in the Heisenberg picture is $\hat{A}(t) = \exp(i\hat{\mathcal{H}}t) \hat{A} \exp(-i\hat{\mathcal{H}}t)$. The Fourier transform of Eq. (2)

$$G_{i\sigma}^r(\omega) \equiv \langle \langle \hat{d}_{i\sigma} : \hat{d}_{i\sigma}^\dagger \rangle \rangle_\omega = \int_{-\infty}^{\infty} G_{i\sigma}^r(t) e^{i\omega t} dt \quad (3)$$

can be directly related to the orbital occupation via ($f \equiv \int \frac{d\omega}{2\pi}$ in the following)

$$\langle \hat{n}_{i\sigma} \rangle = - \int f(\omega) \text{Im} (G_{i\sigma}^r(\omega)), \quad (4)$$

where $f(\omega) = [1 + e^{\beta\omega}]^{-1}$ is the Fermi function.

In order to proceed, it is convenient to introduce a more general GF that represents the GF generated at all orders of the EOM approach:

$$G_B^r(t) = -i\theta(t) \langle \{ \hat{B}(t), \hat{d}_{i\sigma}^\dagger(0) \} \rangle, \quad (5)$$

where the operator $\hat{B}(t)$ is a product of occupation operators multiplied by either a single dot annihilation operator $\hat{d}_{i\sigma}$ or a lead annihilation operator $\hat{c}_{\alpha k i \sigma}$ in the Heisenberg picture. The EOM of its Fourier transform $G_B^r(\omega) \equiv \langle \langle \hat{B} : \hat{d}_{i\sigma}^\dagger \rangle \rangle_\omega$ in the frequency domain can be written as [34, 36, 52]

$$\omega^+ \langle \langle \hat{B} : \hat{d}_{i\sigma}^\dagger \rangle \rangle_\omega = \langle \{ \hat{B}, \hat{d}_{i\sigma}^\dagger \} \rangle + \langle \langle [\hat{B}, \hat{\mathcal{H}}] : \hat{d}_{i\sigma}^\dagger \rangle \rangle_\omega, \quad (6)$$

where $\omega^+ \equiv \omega + i\eta$ with $\eta \rightarrow 0^+$ is the energy ω shifted infinitesimally to the complex plane. We define the general $N + 1$ particle dot GF as $G_{D d_{i\sigma}}^r(\omega) \equiv \langle \langle \hat{D} \hat{d}_{i\sigma} : \hat{d}_{i\sigma}^\dagger \rangle \rangle_\omega$ where $\hat{D} = \hat{n}_{i_1 \sigma_1} \hat{n}_{i_2 \sigma_2} \dots \hat{n}_{i_N \sigma_N}$ with $(i_k, \sigma_k) \neq (i_q, \sigma_q)$ for all $k \neq q$ and $(i_k, \sigma_k) \neq (i\sigma)$ for all $k \in \{1, \dots, N\}$ and $\hat{D} = \hat{1}$ is the unit operator if $N = 0$.

In the following we use the EOM to derive analytical expressions for the dot equilibrium GFs $G_{D d_{i\sigma}}^r(\omega)$ of the DQD system attached to two reservoirs solely in terms of the local occupations $\langle \hat{n}_{i\sigma} \rangle$ and the removal and addition energies of the DQD. Our starting point is the EOM for the retarded single-particle GF

$$\omega^+ \langle \langle \hat{d}_{i\sigma} : \hat{d}_{i\sigma}^\dagger \rangle \rangle_\omega = \langle \{ \hat{d}_{i\sigma}, \hat{d}_{i\sigma}^\dagger \} \rangle + \langle \langle [\hat{d}_{i\sigma}, \hat{\mathcal{H}}] : \hat{d}_{i\sigma}^\dagger \rangle \rangle_\omega. \quad (7)$$

The first term of the right-hand side (r.h.s.) of Eq. (7) directly follows from the anti-commutation rules for creation and annihilation operators: $\langle \{ \hat{d}_{i\sigma}, \hat{d}_{i\sigma}^\dagger \} \rangle = 1$. The

commutator in the second term of the r.h.s. of Eq. (7) is found to be

$$[\hat{d}_{i\sigma}, \hat{\mathcal{H}}] = (v_i + U_i \hat{n}_{i\bar{\sigma}} + U_{12} \hat{n}_{\bar{i}}) \hat{d}_{i\sigma} + \sum_{\alpha k} V_{\alpha k i}^* \hat{c}_{\alpha k i \sigma}, \quad (8)$$

where \bar{i} refers to the site index opposite to i . Hence the second term of the r.h.s. of Eq. (7) generates a contribution to the single-particle GF, two higher order GFs and a mixed dot-lead GF according to:

$$(\omega^+ - v_i) G_{i\sigma}^r(\omega) = 1 + U_i \langle \langle \hat{n}_{i\bar{\sigma}} \hat{d}_{i\sigma} : \hat{d}_{i\sigma}^\dagger \rangle \rangle_\omega + U_{12} \langle \langle \hat{n}_{\bar{i}} \hat{d}_{i\sigma} : \hat{d}_{i\sigma}^\dagger \rangle \rangle_\omega + \sum_{\alpha k} V_{\alpha k i}^* \langle \langle \hat{c}_{\alpha k i \sigma} : \hat{d}_{i\sigma}^\dagger \rangle \rangle_\omega. \quad (9)$$

The EOM of the mixed dot-lead GF is obtained from Eq. (6) with $\hat{B} = \hat{c}_{\alpha k i \sigma}$

$$\omega^+ \langle \langle \hat{c}_{\alpha k i \sigma} : \hat{d}_{i\sigma}^\dagger \rangle \rangle_\omega = \langle \langle [\hat{c}_{\alpha k i \sigma}, \hat{\mathcal{H}}] : \hat{d}_{i\sigma}^\dagger \rangle \rangle_\omega, \quad (10)$$

where the commutator between the annihilation operator of the leads and the Hamiltonian is $[\hat{c}_{\alpha k i \sigma}, \hat{\mathcal{H}}] = \epsilon_{\alpha k i} \hat{c}_{\alpha k i \sigma} + V_{\alpha k i} \hat{d}_{i\sigma}$. Then, the last term of the r.h.s of Eq. (9) becomes

$$\sum_{\alpha k} V_{\alpha k i}^* \langle \langle \hat{c}_{\alpha k i \sigma} : \hat{d}_{i\sigma}^\dagger \rangle \rangle_\omega = \Delta_i(\omega) \langle \langle \hat{d}_{i\sigma} : \hat{d}_{i\sigma}^\dagger \rangle \rangle_\omega, \quad (11)$$

where we have defined the embedding self energy or hybridization function as

$$\Delta_i(\omega) \equiv \sum_{\alpha k} \frac{|V_{\alpha k i}|^2}{\omega^+ - \epsilon_{\alpha k i}}. \quad (12)$$

The hybridization function $\Delta_i(\omega)$ describes the effect of the coupling of QD i to its reservoirs. More specifically, its real part yields the renormalization of the on-site energy v_i , while its imaginary part describes the life-time broadening of the QD level due to the coupling to the reservoirs. Note that due to the fact that each dot only couples to its own left and right leads the embedding self energy is diagonal in the dot indices.

Taking into account the definition of the hybridization function Eq. (12), the single-particle GF can be written as

$$(\omega - v_i - \Delta_i(\omega)) G_{i\sigma}^r(\omega) = 1 + U_i \langle \langle \hat{n}_{i\bar{\sigma}} \hat{d}_{i\sigma} : \hat{d}_{i\sigma}^\dagger \rangle \rangle_\omega + U_{12} \langle \langle \hat{n}_{\bar{i}} \hat{d}_{i\sigma} : \hat{d}_{i\sigma}^\dagger \rangle \rangle_\omega. \quad (13)$$

order GFs thus increases by one.

Setting up the EOMs for the higher order GFs on the r.h.s. of Eq. (13) leads, on the one hand, to the generation of GFs of yet higher order of the form $\langle \langle \hat{n}_{i''\sigma''} \hat{n}_{i'\sigma'} \hat{d}_{i\sigma} : \hat{d}_{i\sigma}^\dagger \rangle \rangle_\omega$. In each subsequent order the number of occupation operators in the generated higher-order GFs thus increases by one. On the other hand, it also generates mixed dot-lead GFs of the same order.

Obviously, we somehow need to truncate the hierarchy of the EOMs.

Below we introduce a truncation scheme, which can be justified in three different ways, all leading to the same result. We first consider the analytic structure of the (dot) GFs of the uncontacted system, which can be written as sums over single poles at certain frequencies shifted infinitesimally from the real axis. The residues of these poles are given by linear combinations of density correlators. A physically plausible model of approximately taking into account the coupling to the leads (and the first way of introducing our truncation scheme) is then given by simply broadening the poles by the embedding self-energies [53–55]. As a second way, the same approximation can also be obtained by neglecting certain GFs, which contain one or more lead operators (for a detailed derivation see Appendix A). Finally, the very same approximate truncation of the EOMs can also be achieved by assuming that the local density operator and the Hamiltonian commute, i.e., $[\hat{n}_{i\sigma}, \hat{\mathcal{H}}] \approx 0$, which becomes exact in the uncontacted situation. The GFs calculated within this approximation are expected to be accurate in the Coulomb blockade (CB) regime, when the temperature kT is large compared to the broadening $-\text{Im}\Delta_i$ by the reservoirs.

Under this approximation, the mixed higher-order GFs are related to the same-order dot GFs via

$$\langle \langle \hat{D} \hat{c}_{\alpha k i \sigma} : \hat{d}_{i\sigma}^\dagger \rangle \rangle_\omega \approx \langle \langle \hat{D} [\hat{c}_{\alpha k i \sigma}, \hat{\mathcal{H}}] : \hat{d}_{i\sigma}^\dagger \rangle \rangle_\omega = \frac{V_{\alpha k i}}{\omega^+ - \epsilon_{\alpha k i}} \langle \langle \hat{D} \hat{d}_{i\sigma} : \hat{d}_{i\sigma}^\dagger \rangle \rangle_\omega. \quad (14)$$

Therefore, the one-body dot GF Eq. (3) can be expressed completely in terms of higher-order dot GFs $G_{Dd_{i\sigma}}^r(\omega)$. Hence, for a finite number of single-particle levels the EOM can be closed at finite order. The EOM approach can thus be solved by recursive evaluation of the EOMs for successive orders of GFs. We can easily see that for the DQD the EOMs can be closed at the fourth order $G_{Dd_{i\sigma}}^r(\omega)$ where $\hat{D} = \hat{n}_{i\bar{\sigma}} \hat{n}_{i\sigma} \hat{n}_{\bar{i}\bar{\sigma}}$, since the additional operator $\hat{n}_{i'\sigma'}$ generated by the interaction part of the EOM must be equal to either one of the operators $\hat{n}_{i\bar{\sigma}}$, $\hat{n}_{i\sigma}$ or $\hat{n}_{\bar{i}\bar{\sigma}}$ in \hat{D} . This yields the four-particle GF

$$\langle \langle \hat{n}_{i\bar{\sigma}} \hat{n}_{i\sigma} \hat{n}_{\bar{i}\bar{\sigma}} \hat{d}_{i\sigma} : \hat{d}_{i\sigma}^\dagger \rangle \rangle_\omega = \frac{\langle \hat{n}_{i\bar{\sigma}} \hat{n}_{i\sigma} \hat{n}_{\bar{i}\bar{\sigma}} \rangle}{\omega - v_i - U_i - 2U_{12} - \Delta_i(\omega)}. \quad (15)$$

As shown in Appendix B, replacing the expressions of the higher-order GFs (expressed in terms of the correlators Eq. (19)) recursively into the lower-order GFs finally allows us to express the one-body GF (3) as

$$G_{i\sigma}^r(\omega) = \sum_{j=1}^6 \frac{r_{i,j}}{\omega - p_{i,j} - \Delta_i(\omega)}, \quad (16)$$

where in order to simplify the notation, we have introduced the following abbreviations for the addition and

removal energies, which define the poles of the GF (16):

$$p_{i,1} = v_i , \quad (17a)$$

$$p_{i,2} = v_i + U_i , \quad (17b)$$

$$p_{i,3} = v_i + U_i + U_{12} , \quad (17c)$$

$$p_{i,4} = v_i + U_i + 2U_{12} , \quad (17d)$$

$$p_{i,5} = v_i + U_{12} , \quad (17e)$$

$$p_{i,6} = v_i + 2U_{12} . \quad (17f)$$

Importantly, the residues $r_{i,j}$ in Eq. (16) can be expressed by linear combinations of the one-, two-, and three-body correlators as follows:

$$r_{i,1} = 1 - \langle \hat{n}_{i\sigma} \rangle - 2 \langle \hat{n}_{i\bar{\sigma}} \rangle + \langle \hat{n}_{i\sigma} \hat{n}_{i\bar{\sigma}} \rangle + 2 \langle \hat{n}_{i\bar{\sigma}} \hat{n}_{i\bar{\sigma}} \rangle - \langle \hat{n}_{i\bar{\sigma}} \hat{n}_{i\bar{\sigma}} \hat{n}_{i\sigma} \rangle , \quad (18a)$$

$$r_{i,2} = \langle \hat{n}_{i\sigma} \rangle - 2 \langle \hat{n}_{i\bar{\sigma}} \hat{n}_{i\bar{\sigma}} \rangle + \langle \hat{n}_{i\bar{\sigma}} \hat{n}_{i\bar{\sigma}} \hat{n}_{i\sigma} \rangle , \quad (18b)$$

$$r_{i,3} = 2(\langle \hat{n}_{i\bar{\sigma}} \hat{n}_{i\bar{\sigma}} \rangle - \langle \hat{n}_{i\bar{\sigma}} \hat{n}_{i\bar{\sigma}} \hat{n}_{i\sigma} \rangle) , \quad (18c)$$

$$r_{i,4} = \langle \hat{n}_{i\bar{\sigma}} \hat{n}_{i\bar{\sigma}} \hat{n}_{i\sigma} \rangle , \quad (18d)$$

$$r_{i,5} = 2(\langle \hat{n}_{i\bar{\sigma}} \rangle - \langle \hat{n}_{i\bar{\sigma}} \hat{n}_{i\bar{\sigma}} \rangle - \langle \hat{n}_{i\bar{\sigma}} \hat{n}_{i\bar{\sigma}} \rangle + \langle \hat{n}_{i\bar{\sigma}} \hat{n}_{i\bar{\sigma}} \hat{n}_{i\sigma} \rangle) , \quad (18e)$$

$$r_{i,6} = \langle \hat{n}_{i\bar{\sigma}} \hat{n}_{i\bar{\sigma}} \rangle - \langle \hat{n}_{i\bar{\sigma}} \hat{n}_{i\bar{\sigma}} \hat{n}_{i\sigma} \rangle . \quad (18f)$$

Eq. (16) provides the structure of the one body GF as a sum of single poles, broadened by the imaginary part of the hybridization function Δ_i . In the wide-band limit (WBL) the hybridization function becomes constant and purely imaginary, $\Delta_i = -i\gamma_i/2$, with $\gamma_i = \gamma_{i,L} + \gamma_{i,R}$. In the following we consider that $\gamma = \gamma_1 = \gamma_2$. We emphasize that also the higher-order dot GFs have a similar structure as Eq. (16) but in this case only a subset of the poles of Eq. (17) contribute, see Appendix B. The imaginary contribution in the denominators is obtained under the approximation $[\hat{n}_{i\sigma}, \hat{\mathcal{H}}] = 0$ and it formally justifies the usual phenomenological procedure in which γ is introduced as a decay parameter in order to broaden the poles of the spectral function for different impurity systems [53–55].

The second step in our analytical EOM approach rests on the observation that one can obtain the static N -body correlator from the GF via [34, 56]

$$\langle \hat{D} \hat{n}_{i\sigma} \rangle = - \int f(\omega) \text{Im} (G_{Dd_{i\sigma}}^r(\omega)) . \quad (19)$$

Since the GFs $G_{Dd_{i\sigma}}^r(\omega)$ only depend *linearly* on the correlators, application of Eq. (19) for all GFs then leads to a linear system for the correlators. Importantly, the fourth-order correlator $\langle \hat{n}_{1\sigma} \hat{n}_{1\bar{\sigma}} \hat{n}_{2\sigma} \hat{n}_{2\bar{\sigma}} \rangle$ does not explicitly appear in the resulting linear system, which thus in principle consists of 15 equations for 15 independent correlators.

The size of the linear system can be reduced due to the spin symmetry in our model (the on-site energies v_i are independent of spin), which reduces the number of independent correlators from 15 to 7 (see Appendix

C). Incidentally, in the method of rate equations [57–59] one solves for the same number of independent variables, which in this case are the probabilities for a certain distribution of occupation numbers in the double dot. In fact, we expect the rate equation approach to be physically equivalent to the EOM approach at our level of approximate treatment of the coupling to the leads.

Another important simplification arises from the fact that all GFs have the analytic structure of a sum of single poles in the complex plane and therefore each integral arising on the r.h.s. of Eq. (19) has the same structure and can be evaluated analytically [47, 60]

$$\begin{aligned} \phi(p) &= \int f(\omega) \frac{\gamma}{(\omega - p)^2 + \frac{\gamma^2}{4}} \\ &= \frac{1}{2} - \frac{1}{\pi} \psi \left(\frac{1}{2} + \frac{\gamma/2 + ip}{2\pi T} \right) , \end{aligned} \quad (20)$$

where $\psi(z) = \frac{d \log(\Gamma(z))}{dz}$ is the digamma function with general complex argument z , and $\Gamma(z)$ is the gamma function. For instance, the two-body correlator function $\langle \hat{n}_{i\bar{\sigma}} \hat{n}_{i\bar{\sigma}} \rangle$, can be expressed as

$$\begin{aligned} \langle \hat{n}_{i\bar{\sigma}} \hat{n}_{i\bar{\sigma}} \rangle &= - \int f(\omega) \text{Im} \left(\langle \langle \hat{n}_{i\bar{\sigma}} \hat{d}_{i\bar{\sigma}} : \hat{d}_{i\bar{\sigma}}^\dagger \rangle \rangle \right) \\ &= \phi(p_{i,5}) (\langle \hat{n}_{i\bar{\sigma}} \rangle - \langle \hat{n}_{i\bar{\sigma}} \hat{n}_{i\bar{\sigma}} \rangle - \langle \hat{n}_{i\bar{\sigma}} \hat{n}_{i\bar{\sigma}} \rangle + \langle \hat{n}_{i\bar{\sigma}} \hat{n}_{i\bar{\sigma}} \hat{n}_{i\sigma} \rangle) \\ &\quad + \phi(p_{i,6}) (\langle \hat{n}_{i\bar{\sigma}} \hat{n}_{i\bar{\sigma}} \rangle - \langle \hat{n}_{i\bar{\sigma}} \hat{n}_{i\bar{\sigma}} \hat{n}_{i\sigma} \rangle) \\ &\quad + \phi(p_{i,3}) (\langle \hat{n}_{i\bar{\sigma}} \hat{n}_{i\bar{\sigma}} \rangle - \langle \hat{n}_{i\bar{\sigma}} \hat{n}_{i\bar{\sigma}} \hat{n}_{i\sigma} \rangle) \\ &\quad + \phi(p_{i,4}) \langle \hat{n}_{i\bar{\sigma}} \hat{n}_{i\bar{\sigma}} \hat{n}_{i\sigma} \rangle . \end{aligned} \quad (21)$$

In other words, *all* coefficients in the linear system for the correlators can be computed analytically. Of course, once these coefficients are known, the resulting linear system can readily be solved numerically. However, in the case of our double dot one can even solve the whole linear system analytically. To this end, for the quantum dot with label i we first solve the subsystem for the higher-order correlators $\langle \hat{n}_{i\bar{\sigma}} \hat{n}_{i\bar{\sigma}} \rangle$, $\langle \hat{n}_{i\bar{\sigma}} \hat{n}_{i\bar{\sigma}} \rangle$, $\langle \hat{n}_{i\bar{\sigma}} \hat{n}_{i\bar{\sigma}} \hat{n}_{i\sigma} \rangle$, and $\langle \hat{n}_{i\bar{\sigma}} \hat{n}_{i\bar{\sigma}} \hat{n}_{i\sigma} \rangle$ and express them in terms of the occupations $\langle \hat{n}_{i\sigma} \rangle = n_{i\sigma}/2$, and $\langle \hat{n}_{i\bar{\sigma}} \rangle = n_{i\bar{\sigma}}/2$. Subsequently, we solve the resulting system for the two local occupations (see Appendix C for the full derivation).

The higher-order correlators are expressed in terms of the occupations as

$$\langle \hat{n}_{i\bar{\sigma}} \hat{n}_{i\bar{\sigma}} \rangle = \tau_{i,1} \langle \hat{n}_{i\bar{\sigma}} \rangle , \quad (22a)$$

$$\langle \hat{n}_{i\bar{\sigma}} \hat{n}_{i\bar{\sigma}} \rangle = \tau_{i,2} \langle \hat{n}_{i\bar{\sigma}} \rangle , \quad (22b)$$

$$\langle \hat{n}_{i\bar{\sigma}} \hat{n}_{i\bar{\sigma}} \hat{n}_{i\sigma} \rangle = \tau_{i,3} \langle \hat{n}_{i\bar{\sigma}} \rangle , \quad (22c)$$

$$\langle \hat{n}_{i\bar{\sigma}} \hat{n}_{i\bar{\sigma}} \hat{n}_{i\sigma} \rangle = \tau_{i,4} \langle \hat{n}_{i\bar{\sigma}} \rangle , \quad (22d)$$

where the parameters $\tau_{i,j}$ are defined in Eq. (C10) and are fully given in terms of the model parameters. Substituting Eq. (22) into Eq. (18) allows us to express the residues of the single-particle GF in terms of the orbital

occupations

$$r_{i,1} = 1 - n_i/2 + (\tau_{i,1} + 2\tau_{i,2} - \tau_{i,3} - 2)n_{\bar{i}}/2, \quad (23a)$$

$$r_{i,2} = n_i/2 + (\tau_{i,3} - 2\tau_{i,2})n_{\bar{i}}/2, \quad (23b)$$

$$r_{i,3} = (\tau_{i,2} - \tau_{i,3})n_{\bar{i}}, \quad (23c)$$

$$r_{i,4} = \tau_{i,3}n_{\bar{i}}/2, \quad (23d)$$

$$r_{i,5} = (1 - \tau_{i,1} - \tau_{i,2} + \tau_{i,3})n_{\bar{i}}, \quad (23e)$$

$$r_{i,6} = (\tau_{i,1} - \tau_{i,3})n_{\bar{i}}/2. \quad (23f)$$

Combining Eqs. (4), (16) and (23) one then arrives at a 2×2 linear system for the local occupations which is readily solved analytically, see Appendix C. The resulting local occupations are then given by:

$$n_i = 2 \frac{\phi(v_i)\eta_{\bar{i}\bar{i}} - \phi(v_{\bar{i}})\eta_{i\bar{i}}}{\eta_{11}\eta_{22} - \eta_{12}\eta_{21}}, \quad (24)$$

where

$$\eta_{ii} = 1 + \phi(p_{i,1}) - \phi(p_{i,2}), \quad (25a)$$

$$\begin{aligned} \eta_{\bar{i}\bar{i}} = & \phi(p_{i,1})(2 + \tau_{i,3} - \tau_{i,1} - 2\tau_{i,2}) + \phi(p_{i,2})(2\tau_{i,2} - \tau_{i,4}) \\ & + 2\phi(p_{i,3})(\tau_{i,3} - \tau_{i,2}) - \tau_{i,3}\phi(p_{i,4}) \\ & + 2\phi(p_{i,5})(\tau_{i,1} + \tau_{i,2} - \tau_{i,3} - 1) + \phi(p_{i,6})(\tau_{i,3} - \tau_{i,1}). \end{aligned} \quad (25b)$$

Eqs. (16), (23) and (24) represent the main results of this work, providing analytical expressions for the evaluation of the Green's functions and the orbital occupations as functions of the model parameters.

In the uncontacted limit $\gamma \rightarrow 0$, our method involves no approximations and treats interactions exactly. The imaginary part of the resulting GF (Eq. (16)) is proportional to a sum of delta functions at frequencies coinciding with the poles $p_{i,j}$ which allows us to express the correlators in terms of Fermi functions, $\phi(p) = f(p)$. The results in this limit are in complete agreement with the grand canonical ensemble (GCE) as it should be.

A common alternative approach to treat the coupling dependence consists in truncating the mixed GFs hierarchy at the level of the two-particle GF, considering the Hubbard-I [35] decoupling $\langle\langle \hat{n}_{i'\sigma'} \hat{c}_{ik\sigma} : d_{i\sigma}^\dagger \rangle\rangle \approx \langle\langle \hat{n}_{i'\sigma'} \rangle\rangle \langle\langle \hat{c}_{ik\sigma} : d_{i\sigma}^\dagger \rangle\rangle$ and treating the inter-dot Coulomb interaction within the Hartree approximation. This method (denoted as EOM-H in the following) has already been explored in the literature [46] and the resulting one-particle GF is

$$\begin{aligned} G_{i\sigma}^r(\omega) = & \frac{1 - n_i/2}{\omega - p_{i,1} - U_{12}n_{\bar{i}} - \Delta_i \left(1 + \frac{U_i n_i/2}{\omega - p_{i,2}}\right)} \\ & + \frac{n_i/2}{\omega - p_{i,2} - U_{12}n_{\bar{i}} - \Delta_i \left(1 - \frac{U_i(1-n_i/2)}{\omega - p_{i,1}}\right)}. \end{aligned} \quad (26)$$

Note that since the spectral function related to Eq. (26) can not be written as a sum of Lorentzian functions, the resulting integrals for obtaining the occupations have to

be solved numerically. Furthermore, the resulting system of equations is nonlinear in the occupations which cannot be solved analytically and requires a numerical approach.

III. RESULTS

In this section, we apply our analytical EOM approach to compute spectral functions and orbital occupations for the DQD in different regimes defined by the interaction parameters (c.f. Ref. 61). We benchmark the results with two well-known numerical methods, namely the non-crossing approximation (NCA) [29, 30] and the hierarchical equations of motion (HEOM) approach [62–64]. A Python code implementing our EOM approach for the DQD is publicly available at GitHub [65].

In the following we consider the three different regimes of interaction parameters U_1 , U_2 , and U_{12} identified in Ref. 61: In Regime I the inter-dot interaction is smaller than either of the intra-dot interactions. Without loss of generality we may also assume $U_2 \leq U_1$, and hence $U_{12} \leq U_2 \leq U_1$. Regime I is the most common (or natural) case, since in physical systems usually the inter-dot (or inter-orbital) interaction will be smaller than the intra-dot (or intra-orbital) ones. On the other hand, Regimes II ($(U_1+U_2)/2 > U_{12} > U_2$) and III ($U_{12} > (U_1+U_2)/2 > U_2$) where U_{12} is larger than at least one of the on-site interactions U_i could be relevant in specific setups or for effective model Hamiltonians.

In order to better understand the structure of the GF given by Eq. (16), in Fig. 1 we plot the residues given by Eq. (23) for QD $i = 1$ as functions of the gate potentials v_i of both QDs for each of the three aforementioned regimes, together with so-called stability diagrams structure (shown as dashed gray lines) in the limit of low coupling and both low (top panels) and higher (bottom panels) temperatures (on the scale of the interactions). A stability diagram is a map of the dot occupation numbers $\{n_1, n_2\}$ as a function of the gate potentials $\{v_1, v_2\}$. It thus shows the regions where the occupation numbers are stable, i.e., do not fluctuate in the limit of low temperature and weak coupling to the reservoirs. Specifically in this limit and for the case of only density-density interactions as in our case, the occupations in the different regions are stable at integer values. As explained in detail in Ref. 61, each regime is characterized by a distinctive stability diagram.

Regime I, shown in Fig. 1(a), is characterized by relatively independent behavior of both dots and a wide central region of occupations (1, 1). In Regime II, shown in Fig. 1(b), the width of the (1, 1) region in the stability diagram is notably reduced, leading to increased regions of the (1, 2) and (2, 1) occupation. Finally, in Regime III, shown in Fig. 1(c), the (1, 1) region of occupations is not present anymore, and the regions (0, 1) and (2, 0) as well as the regions (1, 0) and (0, 2) become adjacent.

We now focus on a given regime, i.e., fixed interactions U_1 , U_2 and U_{12} , and a given region in the $v_1 - v_2$

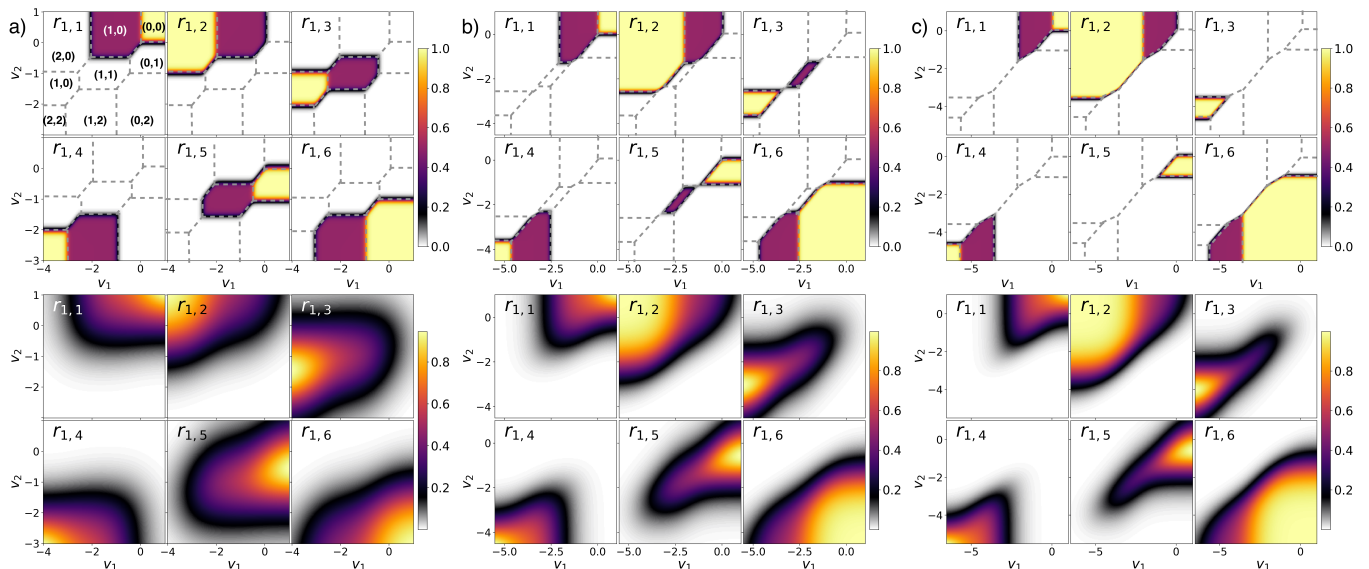


FIG. 1. Green's function residues $r_{1,j}$ of Eq. (23) as a function of the gate potentials for different combinations of the interaction parameters at $T = 0.05$ (top panels) and $T = 0.5$ (bottom panels) in the limit $\gamma \rightarrow 0$. The Coulomb interactions are: (left) $U_1 = 2$ and $U_{12} = 0.5$, (center) $U_1 = 2$ and $U_{12} = 1.3$, and (right) $U_1 = 2$ and $U_{12} = 1.8$. Energies given in units of U_2 .

plane. By inspection of the top panels of Fig. 1 (low coupling and low temperature), we realize that for each given region there are two situations possible: (i) there exists only one non-vanishing residue with value 1 or (ii) there exist two non-vanishing residues both with value 0.5, i.e., the local spectral function (on dot 1) has either one or two poles. In the first case the single pole is at an electron removal or electron addition energy for an electron at the given site. In the case of two poles, the corresponding site is half filled and one can both add and remove an electron to/from that site. Note that both poles have equal spectral weight, i.e., equal residues, because the dot Hamiltonian only contains density-density interactions. As the temperature is increased, eigenstates different from the ground state start to contribute to the ensemble of the dot, and thus more than two poles may contribute to the local spectral function, as can be seen in the bottom panels of Fig. 1 (higher temperature).

In Fig. 2, the total spectral function $A(\omega) = -\text{Im}[G_1^r(\omega) + G_2^r(\omega)]/\pi$ obtained from the analytical EOM, is plotted as a function of the inter-dot Coulomb repulsion U_{12} at the particle-hole symmetric point $v_i = -U_i/2 - U_{12}$, with $T/\gamma = 5$, $U_2 = 1$, and (a) $U_1 = 2/3$ and (b) $U_1 = 0$. The main structure of the spectral function consists of a series of intersecting vertical and diagonal lines. The vertical lines are located at $\omega = \pm U_i/2$ while the diagonals follow from $\pm\omega = \pm U_i/2 - U_{12}$ consistent with the position of the poles Eq. (17) for $v_i = -U_i/2 - U_{12}$.

An important observation is that for small U_{12} values, almost all the spectral weight is carried by the vertical lines. As U_{12} increases, the spectral weight shifts to the diagonal lines. This occurs at the transitions to regime

II (at (panel a) $U_{12} = 2/3$ and to regime III (at (panel a) $U_{12} = 5/6$ and (panel b) $U_{12} = 1/2$). The lines with less spectral weights are due to excited states and their weight decreases in the limit of both $T \rightarrow 0$ and $\gamma \rightarrow 0$ (not shown).

In Fig. 3, we compare our results for the total spectral function (EOM) for those values of U_{12} marked by the green dashed lines in Fig. 2 against three other methods: the Hubbard I + Hartree decoupling scheme of Eq. (26) (EOM-H), NCA, and HEOM for tier level $L = 3$. At small U_{12} values, the EOM-H approach captures the general distribution of the spectral functions (corresponding to the vertical lines in Fig. 2) in comparison to NCA and HEOM. However, as U_{12} increases, EOM-H fails to capture the correct spectral weights of the different peaks, finding that the vertical lines still carry all the spectral weight (instead of the diagonal ones). As shown, the analytical EOM accurately reproduces the position of all the peaks and correctly captures the spectral weight distributions for all values of U_{12} .

Finally, in the left columns of Fig. 4 we present a comparison of the local occupations as a function of the average gate level $v = (v_1 + v_2)/2$ between our analytical EOM approach, the EOM-H approximation and the HEOM method for different interactions and $\delta v = v_1 - v_2$, at a fixed $T = 2\gamma = 0.1$. In panel a) with $U_1 = 0.75$, the local occupations are degenerate up to half occupation at $v \sim -0.5$. Then, n_1 evolves faster to full occupation due to the smaller intra-dot Coulomb repulsion. In panel b) where a finite energy difference is applied between the gate levels, $\delta v = v_1 - v_2 = 0.5$, the occupation of site one is shifted to lower gates, with two plateaus close to half filling being the main features of the densities. In

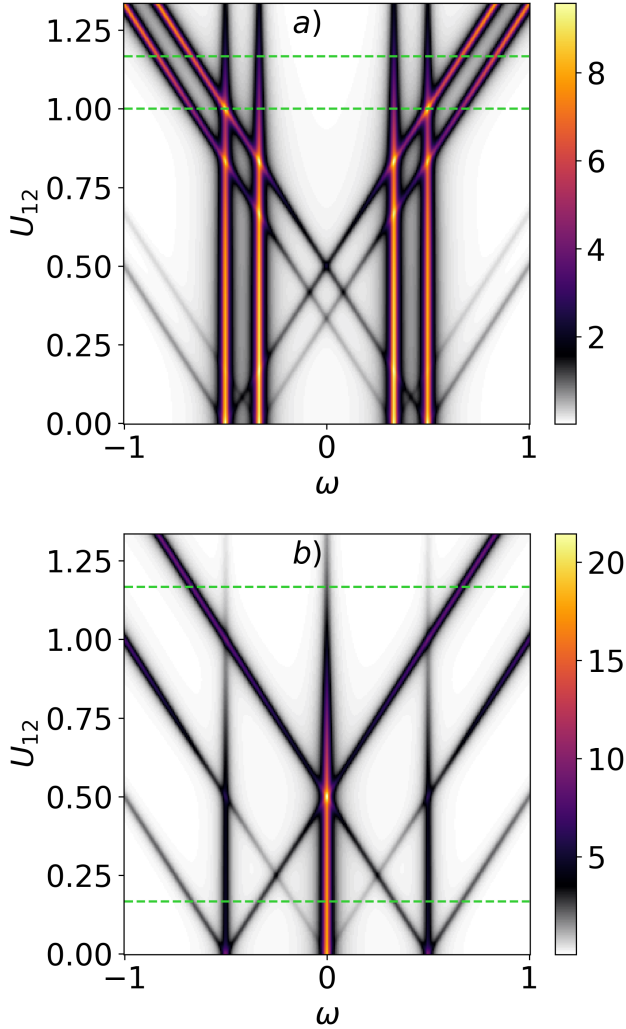


FIG. 2. Spectral function of the double quantum dot from Eqs. (16) and (23) for $T = 1/6$, $\gamma = 1/30$ at the particle-hole symmetric point $v_i = -U_i/2 - U_{12}$. (a) $U_1 = 2/3$ and (b) $U_1 = 0$. Energies in units of U_2 .

panel c) where $U_1 = 0.5$ and $\delta v = 0$, both n_i evolve together as the gate is decreased up to quarter occupation at $v \sim 0$. As in a), then n_1 evolves faster to full occupation. Finally, in in panel d), the local occupation of site one is shifted to lower gate levels v . In all the situations studied with $T/\gamma > 1$, the agreement between the EOM approach and the HEOM is excellent, with our analytical EOM approach accurately capturing the local step structures due to the interactions and the corresponding slopes governed by the combination of temperature and coupling strength. On the other hand, although the EOM-H approximation captures the general trend of the local occupations, it fails to accurately predict some local transitions. In particular, the EOM-H approximation does not correctly capture the new plateaus at non-integer values of the local occupations observed in the

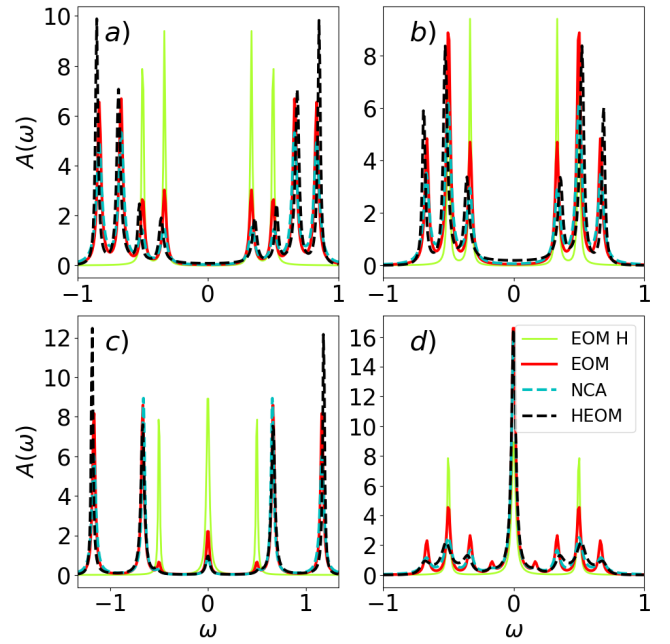


FIG. 3. Spectral function of the double quantum dot at $T = 1/6$, $\gamma = 1/30$ and at the particle-hole symmetric point $v_i = -U_i/2 - U_{12}$. In (a) $U_1 = 2/3$, $U_{12} = 7/6$, (b) $U_1 = 2/3$, $U_{12} = 1$, (c) $U_1 = 0$, $U_{12} = 7/6$, and (d) $U_1 = 0$, $U_{12} = 1/6$. The different lines correspond to the EOM Hartree approximation (EOM-H) (divided by 2 for representation clarity), the analytical EOM of Eqs. (16) and (23), and the numerical results from NCA and HEOM. Energies in units of U_2 .

EOM and HEOM results. This discrepancy highlights the limitation of the EOM-H method in dealing with the inter-dot Coulomb repulsion, not recovering correctly the GCE limit (not shown).

The right panels in Fig. 4 depict the spectral functions corresponding to each case on the left as a function of the average gate v . As expected, all non-vanishing spectral features depend linearly on v due to the positions of the poles given by $\omega = p_{i,j}$. The weight of each contribution (given by the residues) varies as the interaction changes, but at full occupation, all the spectral weight is carried by $r_{i,4}$ since in this case one can only remove an electron with a removal energy given by $p_{i,4}$. In the empty dot case, all the weight is carried by the residue $r_{i,1}$, since now one can only add an electron with an addition energy given by $p_{i,1}$.

IV. CONCLUSIONS

In this paper, we have introduced a fully analytical EOM approach to analyze the spectral properties and orbital occupations of an interacting DQD system connected to leads. A critical aspect of our approach is the systematic closure of the hierarchy of higher-order GFs, which arises from a consistent approximate treatment of

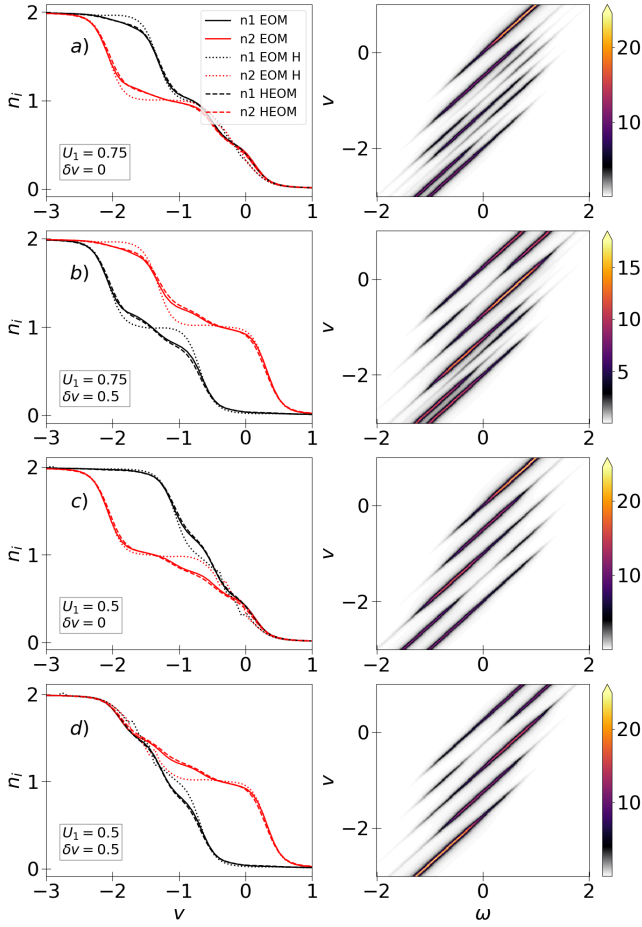


FIG. 4. Local occupations (left) and spectral functions (right) as function of the average gate level $v = (v_1 + v_2)/2$ for $U_{12} = 0.5$, $T = 0.1$, and $\gamma = 0.05$. The other interaction and parameters are (a) $U_1 = 0.75$ and $\delta v = 0$, (b) $U_1 = 0.75$ and $\delta v = 0.5$, (c) $U_1 = 0.5$ and $\delta v = 0$, and (d) $U_1 = 0.5$ and $\delta v = 0.5$. Energies in units of U_2 .

the coupling to the leads for the GFs at all orders. This closure is essential to map the EOMs for the GFs onto a linear system for the density correlators, a mapping that can be applied to any number of levels. For our double dot system it allows us to derive tractable analytical expressions for the one-body GF in terms of the local occupations and all the model parameters. In the low coupling limit, our method correctly recovers the results of the grand canonical ensemble, further validating the approach.

We compared our analytical results with those obtained from the NCA and the HEOM methods. Our approach accurately reproduces the spectral peak positions and weight distributions, demonstrating its effectiveness in capturing the essential physics of the strongly correlated electron system in the Coulomb blockade regime. The agreement with these established numerical techniques underscores the reliability of our approach.

The analytical EOM approach offers substantial ad-

vantages, including explicit functional dependencies that provide insights into the physical mechanisms governing the system. Furthermore, the computational efficiency of our analytical method enables a cheap exploration of different parameter regimes of the system and the study of properties such as the transport coefficients. Additionally, this computational efficiency may be particularly beneficial for, e.g., density functional theory and its extensions, where knowledge of the many-body spectral function in analytic form can be of crucial importance for the construction of the exchange-correlation potentials by reverse engineering.[66–70].

Appendix A: Approximate treatment of coupling to leads

The purpose of the present Appendix is to treat the coupling to the leads directly from the EOM and highlight the approximations which lead to the contribution of the standard embedding self energy of Eq. (12) in both the single-particle and higher order GFs (which in the WBL leads to simple broadening of all poles of the GFs by the wide-band parameter γ used in Sec. II).

In Sec. II we have defined the Green function $\langle\langle \hat{D} \hat{d}_{i\sigma} : \hat{d}_{i\sigma}^\dagger \rangle\rangle_\omega$ with the operator $\hat{D} = \hat{n}_{i_1\sigma_1} \hat{n}_{i_2\sigma_2} \dots \hat{n}_{i_N\sigma_N}$ being a product of N density operators with $(i_k\sigma_k) \neq (i\sigma)$ for all $k \in \{1, \dots, N\}$. In addition, for $N = 0$ we define $\hat{D} = \hat{1}$ as the unit operator. We note that $\hat{d}_{i\sigma}$ commutes with \hat{D} for all N , i.e., $[\hat{D}, \hat{d}_{i\sigma}] = [\hat{D}, \hat{d}_{i\sigma}^\dagger] = 0$.

After straightforward, if somewhat tedious calculations one obtains the EOM for $\langle\langle \hat{D} \hat{d}_{i\sigma} : \hat{d}_{i\sigma}^\dagger \rangle\rangle_\omega$ which reads

$$\begin{aligned}
 & (\omega - v_i) \langle\langle \hat{D} \hat{d}_{i\sigma} : \hat{d}_{i\sigma}^\dagger \rangle\rangle_\omega \\
 &= \langle \hat{D} \rangle + U_i \langle\langle \hat{D} \hat{n}_{i\bar{\sigma}} \hat{d}_{i\sigma} : \hat{d}_{i\sigma}^\dagger \rangle\rangle_\omega \\
 &+ \sum_{j\sigma'} U_{ij} \langle\langle \hat{D} \hat{n}_{j\sigma'} \hat{d}_{i\sigma} : \hat{d}_{i\sigma}^\dagger \rangle\rangle_\omega \\
 &+ \sum_k V_{\alpha ki}^* \langle\langle \hat{D}_N \hat{c}_{\alpha k i\sigma} : \hat{d}_{i\sigma}^\dagger \rangle\rangle_\omega \\
 &+ \sum_{j\alpha k\sigma'} V_{\alpha kj}^* \langle\langle [\hat{d}_{j\sigma'}^\dagger, \hat{D}] \hat{d}_{i\sigma} \hat{c}_{\alpha k j\sigma'} : \hat{d}_{i\sigma}^\dagger \rangle\rangle_\omega \\
 &+ \sum_{j\alpha k\sigma'} V_{\alpha kj} \langle\langle \hat{c}_{\alpha k j\sigma'}^\dagger [\hat{d}_{j\sigma'}, \hat{D}] \hat{d}_{i\sigma} : \hat{d}_{i\sigma}^\dagger \rangle\rangle_\omega. \quad (\text{A1})
 \end{aligned}$$

Similarly, the EOM for the mixed dot-lead GF $\langle\langle \hat{D} \hat{c}_{\alpha k i\sigma} : \hat{d}_{i\sigma}^\dagger \rangle\rangle_\omega$ reads

$$\begin{aligned}
 & (\omega - \epsilon_{\alpha ki}) \langle\langle \hat{D} \hat{c}_{\alpha k i\sigma} : \hat{d}_{i\sigma}^\dagger \rangle\rangle_\omega \\
 &= V_{\alpha ki} \langle\langle \hat{D} \hat{d}_{i\sigma} : \hat{d}_{i\sigma}^\dagger \rangle\rangle_\omega \\
 &+ \sum_{j\alpha'q\sigma'} V_{\alpha'qj}^* \langle\langle [\hat{D}, \hat{d}_{j\sigma'}^\dagger] \hat{c}_{\alpha'qj\sigma'} \hat{c}_{\alpha k i\sigma} : \hat{d}_{i\sigma}^\dagger \rangle\rangle_\omega \\
 &+ \sum_{j\alpha'q\sigma'} V_{\alpha'qj} \langle\langle \hat{c}_{\alpha'qj\sigma'}^\dagger \hat{c}_{\alpha k i\sigma} [\hat{d}_{j\sigma'}, \hat{D}] : \hat{d}_{i\sigma}^\dagger \rangle\rangle_\omega \quad (\text{A2})
 \end{aligned}$$

If in Eqs. (A1) and (A2) we make the approximations

$$\begin{aligned} \langle\langle [\hat{d}_{j\sigma'}^\dagger, \hat{D}] \hat{d}_{i\sigma} \hat{c}_{\alpha k i \sigma'} : \hat{d}_{i\sigma}^\dagger \rangle\rangle_\omega &\approx 0, \\ \langle\langle \hat{c}_{\alpha k i \sigma'}^\dagger [\hat{d}_{j\sigma'}, \hat{D}] \hat{d}_{i\sigma} : \hat{d}_{i\sigma}^\dagger \rangle\rangle_\omega &\approx 0, \\ \langle\langle [\hat{D}, \hat{d}_{j\sigma'}^\dagger] \hat{c}_{\alpha' q j \sigma'} \hat{c}_{\alpha k i \sigma} : \hat{d}_{i\sigma}^\dagger \rangle\rangle_\omega &\approx 0, \\ \langle\langle \hat{c}_{\alpha' q j \sigma'}^\dagger \hat{c}_{\alpha k i \sigma} [\hat{d}_{j\sigma'}, \hat{D}] : \hat{d}_{i\sigma}^\dagger \rangle\rangle_\omega &\approx 0, \end{aligned} \quad (\text{A3})$$

insert the resulting Eq. (A2) into (A1) and obtain

$$\begin{aligned} (\omega - v_i - \Delta_i(\omega)) \langle\langle \hat{D} \hat{d}_{i\sigma} : \hat{d}_{i\sigma}^\dagger \rangle\rangle_\omega \\ = \langle\hat{D}\rangle + U_i \langle\langle \hat{D} \hat{n}_{i\bar{\sigma}} \hat{d}_{i\sigma} : \hat{d}_{i\sigma}^\dagger \rangle\rangle_\omega \\ + \sum_{j\sigma'} U_{ij} \langle\langle \hat{D} \hat{n}_{j\sigma'} \hat{d}_{i\sigma} : \hat{d}_{i\sigma}^\dagger \rangle\rangle_\omega. \end{aligned} \quad (\text{A4})$$

We note that for the single-particle GF, the approximation of Eq. (A3) becomes exact and we obtain Eq. (13).

Appendix B: Green functions

Since Eq. (1) is time-independent, the equation of motion of a general Green's function $\langle\langle \hat{B}(t) : \hat{d}_{i\sigma}^\dagger(0) \rangle\rangle$ can be expressed in the frequency domain through the relation [52]

$$\omega \langle\langle \hat{B} : \hat{d}_{i\sigma}^\dagger \rangle\rangle_\omega = \langle\{\hat{B}, \hat{d}_{i\sigma}^\dagger\}\rangle + \langle\langle [\hat{B}, \hat{\mathcal{H}}] : \hat{d}_{i\sigma}^\dagger \rangle\rangle_\omega. \quad (\text{B1})$$

The one body GF $\langle\langle \hat{d}_{i\sigma} : \hat{d}_{i\sigma}^\dagger \rangle\rangle_\omega$ is then derived from

$$\omega \langle\langle \hat{d}_{i\sigma} : \hat{d}_{i\sigma}^\dagger \rangle\rangle_\omega = \langle\{\hat{d}_{i\sigma}, \hat{d}_{i\sigma}^\dagger\}\rangle + \langle\langle [\hat{d}_{i\sigma}, \hat{\mathcal{H}}] : \hat{d}_{i\sigma}^\dagger \rangle\rangle_\omega, \quad (\text{B2})$$

with the anti commutation relations for the creation and annihilation operators $\{\hat{d}_{i\sigma}, \hat{d}_{j\sigma}^\dagger\} = \delta_{ij}$, $\{\hat{d}_{i\sigma}, \hat{d}_{j\sigma}\} = \{\hat{d}_{i\sigma}^\dagger, \hat{d}_{j\sigma}^\dagger\} = 0$. The commutator of the annihilation operators in the dots of the DQD Hamiltonian follow

$$[\hat{d}_{i\sigma}, \hat{\mathcal{H}}] = (v_i + U_i \hat{n}_{i\bar{\sigma}} + U_{12} \hat{n}_{\bar{i}}) \hat{d}_{i\sigma} + \sum_{\alpha k} V_{\alpha k i}^* \hat{c}_{\alpha k i \sigma}. \quad (\text{B3})$$

Using Eq. (A4) for $\hat{D} = \hat{1}$, the equation of motion for the single-particle GF reads

$$\begin{aligned} \langle\langle \hat{d}_{i\sigma} : \hat{d}_{i\sigma}^\dagger \rangle\rangle_\omega &= \frac{1}{\omega - v_i - \Delta_i} + \frac{U_i \langle\langle \hat{n}_{i\bar{\sigma}} \hat{d}_{i\sigma} : \hat{d}_{i\sigma}^\dagger \rangle\rangle_\omega}{\omega - v_i - \Delta_i} \\ &+ \frac{U_{12}}{\omega - v_i - \Delta_i} \sum_{\sigma'} \langle\langle \hat{n}_{\bar{i}\sigma'} \hat{d}_{i\sigma} : \hat{d}_{i\sigma}^\dagger \rangle\rangle_\omega. \end{aligned} \quad (\text{B4})$$

The two-body GF $\langle\langle \hat{n}_{i\bar{\sigma}} \hat{d}_{i\sigma} : \hat{d}_{i\sigma}^\dagger \rangle\rangle_\omega$ follows from the evaluation of Eq. (A4) with $\hat{D} = \hat{n}_{i\bar{\sigma}}$ which gives

$$\begin{aligned} \langle\langle \hat{n}_{i\bar{\sigma}} \hat{d}_{i\sigma} : \hat{d}_{i\sigma}^\dagger \rangle\rangle_\omega &= \frac{\langle\hat{n}_{i\bar{\sigma}}\rangle}{\omega - v_i - U_i - \Delta_i} + \\ \sum_{\sigma'} \frac{U_{12}}{\omega - v_i - U_i - \Delta_i} \langle\langle \hat{n}_{i\bar{\sigma}} \hat{n}_{\bar{i}\sigma'} \hat{d}_{i\sigma} : \hat{d}_{i\sigma}^\dagger \rangle\rangle_\omega, \end{aligned} \quad (\text{B5})$$

while the other two two-particle GFs are

$$\begin{aligned} \langle\langle \hat{n}_{i\bar{\sigma}} \hat{d}_{i\sigma} : \hat{d}_{i\sigma}^\dagger \rangle\rangle_\omega &= \frac{\langle\hat{n}_{i\bar{\sigma}}\rangle}{\omega - v_i - U_{12} - \Delta_i} + \\ \frac{U_i \langle\langle \hat{n}_{i\bar{\sigma}} \hat{n}_{\bar{i}\sigma} \hat{d}_{i\sigma} : \hat{d}_{i\sigma}^\dagger \rangle\rangle_\omega}{\omega - v_i - U_{12} - \Delta_i} &+ \frac{U_{12} \langle\langle \hat{n}_{i\bar{\sigma}} \hat{n}_{\bar{i}\sigma} \hat{d}_{i\sigma} : \hat{d}_{i\sigma}^\dagger \rangle\rangle_\omega}{\omega - v_i - U_{12} - \Delta_i}, \end{aligned} \quad (\text{B6})$$

and

$$\begin{aligned} \langle\langle \hat{n}_{\bar{i}\sigma} \hat{d}_{i\sigma} : \hat{d}_{i\sigma}^\dagger \rangle\rangle_\omega &= \frac{\langle\hat{n}_{\bar{i}\sigma}\rangle}{(\omega - v_i - U_{12} - \Delta_i)} + \\ \frac{U_i \langle\langle \hat{n}_{i\bar{\sigma}} \hat{n}_{\bar{i}\sigma} \hat{d}_{i\sigma} : \hat{d}_{i\sigma}^\dagger \rangle\rangle_\omega}{\omega - v_i - U_{12} - \Delta_i} &+ \frac{U_{12} \langle\langle \hat{n}_{i\bar{\sigma}} \hat{n}_{\bar{i}\sigma} \hat{d}_{i\sigma} : \hat{d}_{i\sigma}^\dagger \rangle\rangle_\omega}{\omega - v_i - U_{12} - \Delta_i}. \end{aligned} \quad (\text{B7})$$

Similarly, for the three three-body GFs we obtain

$$\begin{aligned} \langle\langle \hat{n}_{i\bar{\sigma}} \hat{n}_{\bar{i}\sigma} \hat{d}_{i\sigma} : \hat{d}_{i\sigma}^\dagger \rangle\rangle_\omega &= \frac{\langle\hat{n}_{i\bar{\sigma}} \hat{n}_{\bar{i}\sigma}\rangle}{\omega - v_i - U_i - U_{12} - \Delta_i} \\ &+ \frac{U_{12} \langle\langle \hat{n}_{i\bar{\sigma}} \hat{n}_{\bar{i}\sigma} \hat{n}_{\bar{i}\sigma} \hat{d}_{i\sigma} : \hat{d}_{i\sigma}^\dagger \rangle\rangle_\omega}{\omega - v_i - U_i - U_{12} - \Delta_i}, \end{aligned} \quad (\text{B8})$$

$$\begin{aligned} \langle\langle \hat{n}_{\bar{i}\sigma} \hat{n}_{\bar{i}\sigma} \hat{d}_{i\sigma} : \hat{d}_{i\sigma}^\dagger \rangle\rangle_\omega &= \frac{\langle\hat{n}_{\bar{i}\sigma} \hat{n}_{\bar{i}\sigma}\rangle}{\omega - v_i - U_i - U_{12} - \Delta_i} \\ &+ \frac{U_{12} \langle\langle \hat{n}_{i\bar{\sigma}} \hat{n}_{\bar{i}\sigma} \hat{n}_{\bar{i}\sigma} \hat{d}_{i\sigma} : \hat{d}_{i\sigma}^\dagger \rangle\rangle_\omega}{\omega - v_i - U_i - U_{12} - \Delta_i}, \end{aligned} \quad (\text{B9})$$

and

$$\begin{aligned} \langle\langle \hat{n}_{i\bar{\sigma}} \hat{n}_{\bar{i}\sigma} \hat{d}_{i\sigma} : \hat{d}_{i\sigma}^\dagger \rangle\rangle_\omega &= \frac{\langle\hat{n}_{i\bar{\sigma}} \hat{n}_{\bar{i}\sigma}\rangle}{\omega - v_i - U_i - U_{12} - \Delta_i} \\ &+ \frac{U_{12} \langle\langle \hat{n}_{i\bar{\sigma}} \hat{n}_{\bar{i}\sigma} \hat{n}_{\bar{i}\sigma} \hat{d}_{i\sigma} : \hat{d}_{i\sigma}^\dagger \rangle\rangle_\omega}{\omega - v_i - U_i - U_{12} - \Delta_i}. \end{aligned} \quad (\text{B10})$$

Finally, the four-body GF reads

$$\langle\langle \hat{n}_{i\bar{\sigma}} \hat{n}_{\bar{i}\sigma} \hat{n}_{\bar{i}\sigma} \hat{d}_{i\sigma} : \hat{d}_{i\sigma}^\dagger \rangle\rangle_\omega = \frac{\langle\hat{n}_{i\bar{\sigma}} \hat{n}_{\bar{i}\sigma} \hat{n}_{\bar{i}\sigma}\rangle}{\omega - v_i - U_i - 2U_{12} - \Delta_i}. \quad (\text{B11})$$

Eq. (B11) is the highest order GF in the EOM hierarchy. We see that all the GFs depend not only on the parameters of the problem but also on the various density correlators. In order to obtain expressions for the GFs, we start by inserting the four-particle GF of Eq. (B11) into Eqs. (B8)-(B10) for the different three-particle GFs. Using partial fraction decompositions along the way we obtain

$$\begin{aligned} \langle\langle \hat{n}_{i\bar{\sigma}} \hat{n}_{\bar{i}\sigma} \hat{d}_{i\sigma} : \hat{d}_{i\sigma}^\dagger \rangle\rangle_\omega &= \frac{\langle\hat{n}_{i\bar{\sigma}} \hat{n}_{\bar{i}\sigma}\rangle - \langle\hat{n}_{i\bar{\sigma}} \hat{n}_{\bar{i}\sigma} \hat{n}_{\bar{i}\sigma}\rangle}{\omega - v_i - U_i - U_{12} - \Delta_i} \\ &+ \frac{\langle\hat{n}_{i\bar{\sigma}} \hat{n}_{\bar{i}\sigma} \hat{n}_{\bar{i}\sigma}\rangle}{\omega - v_i - U_i - U_{12} - \Delta_i}, \end{aligned} \quad (\text{B12})$$

$$\begin{aligned} \langle\langle \hat{n}_{\bar{i}\sigma} \hat{n}_{\bar{i}\sigma} \hat{d}_{i\sigma} : \hat{d}_{i\sigma}^\dagger \rangle\rangle_\omega &= \frac{\langle\hat{n}_{\bar{i}\sigma} \hat{n}_{\bar{i}\sigma}\rangle - \langle\hat{n}_{i\bar{\sigma}} \hat{n}_{\bar{i}\sigma} \hat{n}_{\bar{i}\sigma}\rangle}{\omega - v_i - U_i - U_{12} - \Delta_i} \\ &+ \frac{\langle\hat{n}_{i\bar{\sigma}} \hat{n}_{\bar{i}\sigma} \hat{n}_{\bar{i}\sigma}\rangle}{\omega - v_i - U_i - U_{12} - \Delta_i}, \end{aligned} \quad (\text{B13})$$

and

$$\begin{aligned} \langle\langle \hat{n}_{i\bar{\sigma}} \hat{n}_{i\bar{\sigma}} \hat{d}_{i\sigma} : \hat{d}_{i\sigma}^\dagger \rangle\rangle_\omega &= \frac{\langle \hat{n}_{i\bar{\sigma}} \hat{n}_{i\bar{\sigma}} \rangle - \langle \hat{n}_{i\bar{\sigma}} n_{i\bar{\sigma}} \hat{n}_{i\bar{\sigma}} \rangle}{\omega - v_i - U_i - U_{12} - \Delta_i} \\ &+ \frac{\langle \hat{n}_{i\bar{\sigma}} n_{i\bar{\sigma}} \hat{n}_{i\bar{\sigma}} \rangle}{\omega - v_i - U_i - U_{12} - \Delta_i}. \end{aligned} \quad (\text{B14})$$

Inserting Eqs. (B12)-(B14) into Eqs. (B5)-(B7) leads to the two-particle GFs

$$\begin{aligned} &\langle\langle \hat{n}_{i\bar{\sigma}} \hat{d}_{i\sigma} : \hat{d}_{i\sigma}^\dagger \rangle\rangle_\omega \\ &= \frac{\langle \hat{n}_{i\bar{\sigma}} \rangle - \langle \hat{n}_{i\bar{\sigma}} \hat{n}_{i\bar{\sigma}} \rangle - \langle \hat{n}_{i\bar{\sigma}} \hat{n}_{i\bar{\sigma}} \rangle + \langle \hat{n}_{i\bar{\sigma}} n_{i\bar{\sigma}} \hat{n}_{i\bar{\sigma}} \rangle}{\omega - v_i - U_i - \Delta_i} \\ &+ \frac{\langle \hat{n}_{i\bar{\sigma}} \hat{n}_{i\bar{\sigma}} \rangle + \langle \hat{n}_{i\bar{\sigma}} \hat{n}_{i\bar{\sigma}} \rangle - 2 \langle \hat{n}_{i\bar{\sigma}} n_{i\bar{\sigma}} \hat{n}_{i\bar{\sigma}} \rangle}{\omega - v_i - U_i - U_{12} - \Delta_i} \\ &+ \frac{\langle \hat{n}_{i\bar{\sigma}} n_{i\bar{\sigma}} \hat{n}_{i\bar{\sigma}} \rangle}{\omega - v_i - U_i - 2U_{12} - \Delta_i}, \end{aligned} \quad (\text{B15})$$

$$\begin{aligned} &\langle\langle \hat{n}_{i\bar{\sigma}} \hat{d}_{i\sigma} : \hat{d}_{i\sigma}^\dagger \rangle\rangle_\omega \\ &= \frac{\langle \hat{n}_{i\bar{\sigma}} \rangle - \langle \hat{n}_{i\bar{\sigma}} \hat{n}_{i\bar{\sigma}} \rangle - \langle \hat{n}_{i\bar{\sigma}} \hat{n}_{i\bar{\sigma}} \rangle + \langle \hat{n}_{i\bar{\sigma}} n_{i\bar{\sigma}} \hat{n}_{i\bar{\sigma}} \rangle}{\omega - v_i - U_{12} - \Delta_i} \\ &+ \frac{\langle \hat{n}_{i\bar{\sigma}} \hat{n}_{i\bar{\sigma}} \rangle - \langle \hat{n}_{i\bar{\sigma}} n_{i\bar{\sigma}} \hat{n}_{i\bar{\sigma}} \rangle}{\omega - v_i - U_i - U_{12} - \Delta_i} + \frac{\langle \hat{n}_{i\bar{\sigma}} \hat{n}_{i\bar{\sigma}} \rangle - \langle \hat{n}_{i\bar{\sigma}} n_{i\bar{\sigma}} \hat{n}_{i\bar{\sigma}} \rangle}{\omega - v_i - 2U_{12} - \Delta_i} \\ &+ \frac{\langle \hat{n}_{i\bar{\sigma}} n_{i\bar{\sigma}} \hat{n}_{i\bar{\sigma}} \rangle}{\omega - v_i - U_i - 2U_{12} - \Delta_i}, \end{aligned} \quad (\text{B16})$$

and

$$\begin{aligned} &\langle\langle \hat{n}_{i\bar{\sigma}} \hat{d}_{i\sigma} : \hat{d}_{i\sigma}^\dagger \rangle\rangle_\omega \\ &= \frac{\langle \hat{n}_{i\bar{\sigma}} \rangle - \langle \hat{n}_{i\bar{\sigma}} \hat{n}_{i\bar{\sigma}} \rangle - \langle \hat{n}_{i\bar{\sigma}} \hat{n}_{i\bar{\sigma}} \rangle + \langle \hat{n}_{i\bar{\sigma}} n_{i\bar{\sigma}} \hat{n}_{i\bar{\sigma}} \rangle}{\omega - v_i - U_{12} - \Delta_i} \\ &+ \frac{\langle \hat{n}_{i\bar{\sigma}} \hat{n}_{i\bar{\sigma}} \rangle - \langle \hat{n}_{i\bar{\sigma}} n_{i\bar{\sigma}} \hat{n}_{i\bar{\sigma}} \rangle}{\omega - v_i - U_i - U_{12} - \Delta_i} + \frac{\langle \hat{n}_{i\bar{\sigma}} \hat{n}_{i\bar{\sigma}} \rangle - \langle \hat{n}_{i\bar{\sigma}} n_{i\bar{\sigma}} \hat{n}_{i\bar{\sigma}} \rangle}{\omega - v_i - 2U_{12} - \Delta_i} \\ &+ \frac{\langle \hat{n}_{i\bar{\sigma}} n_{i\bar{\sigma}} \hat{n}_{i\bar{\sigma}} \rangle}{\omega - v_i - U_i - 2U_{12} - \Delta_i}. \end{aligned} \quad (\text{B17})$$

Finally, in order to obtain the one-particle GF, we insert Eqs. (B15)-(B17) into Eq. (B4) to arrive at Eq. (16). In this very last step we used some of the relations due to the spin symmetry of our problem derived in Appendix C.

Appendix C: Linear system for density correlators and analytic solution

In the previous Appendix we have expressed the GFs in terms of density correlators. The correlators themselves can be obtained from the GFs using Eq. (19). Thus this latter relation allows to derive a linear system for the correlators which can easily be solved numerically. Before deriving this linear system, however, we show that as a consequence of the spin symmetry in our problem, i.e., the fact that the on-site energies v_i are independent of σ , some of the density correlators coincide. This allows to reduce the size of the linear problem and for the case of our double dot even to find a fully analytic solution.

We start by using Eq. (19) on Eq. (B11) with the embedding self energy in the wide-band limit $\Delta_i = -i\frac{\gamma}{2}$. This leads to

$$\langle \hat{n}_{i\sigma} \hat{n}_{i\bar{\sigma}} \hat{n}_{i\bar{\sigma}} \hat{n}_{i\sigma} \rangle = \phi(v_i + U_i + 2U_{12}) \langle \hat{n}_{i\bar{\sigma}} \hat{n}_{i\bar{\sigma}} \hat{n}_{i\bar{\sigma}} \rangle, \quad (\text{C1})$$

where we used the function $\phi(p)$ defined in Eq. (20). For given dot index i the r.h.s. of Eq. (C1) is independent of σ . Since the prefactor $\phi(v_i + U_i + 2U_{12})$ on the l.h.s. of the same equation is not only strictly positive at finite temperature but also independent of σ , we conclude that the three-body correlator $\langle \hat{n}_{i\bar{\sigma}} \hat{n}_{i\bar{\sigma}} \hat{n}_{i\bar{\sigma}} \rangle$ is independent of σ as well.

Using this result and a similar reasoning for Eqs. (B12) and (B14) we find that all two-body correlators of the form $\langle \hat{n}_{1\sigma} \hat{n}_{2\sigma'} \rangle$ are independent of both σ and σ' . The spin symmetry of the two-body and the three-body correlators can in an analogous way be used for Eq. (B15) to find that the spin densities $\langle \hat{n}_{i\sigma} \rangle$ on dot i are independent of σ as expected.

If we use Eq. (19) on Eqs. (B11) - (B17) as well as Eq. (16) for all possible values for the indices but do not make use of the spin symmetry we arrive at a 15×15 linear system for the one-, two-, and three-body correlators. Instead when using the spin symmetry relations derived above, the corresponding linear system reduces to 7×7 thus leading to a significantly reduced complexity. To be explicit, for the vector of density correlators

$$\mathbf{y} = \begin{pmatrix} \langle \hat{n}_1 \rangle \\ \langle \hat{n}_2 \rangle \\ \langle \hat{n}_{1\uparrow} \hat{n}_{1\downarrow} \rangle \\ \langle \hat{n}_{2\uparrow} \hat{n}_{2\downarrow} \rangle \\ \langle \hat{n}_{1\uparrow} \hat{n}_{2\downarrow} \rangle \\ \langle \hat{n}_{1\uparrow} \hat{n}_{1\downarrow} \hat{n}_{2\uparrow} \rangle \\ \langle \hat{n}_{2\uparrow} \hat{n}_{2\downarrow} \hat{n}_{1\uparrow} \rangle \end{pmatrix}, \quad (\text{C2})$$

the linear system we need to solve reads

$$\mathbf{C}\mathbf{y} = \mathbf{b}, \quad (\text{C3})$$

where both the matrix \mathbf{C} and the vector \mathbf{b} are explicitly given in terms of the model parameters as

$$\mathbf{C} = \begin{pmatrix} 1 + \ell_{11} - \ell_{12} & 2(\ell_{11} - \ell_{15}) & 0 & 2\ell_{15} - \ell_{11} - \ell_{16} & 2\zeta_1 & 0 & \nu_1 \\ 2(\ell_{21} - \ell_{25}) & 1 + \ell_{21} - \ell_{22} & 2\ell_{25} - \ell_{21} - \ell_{26} & 0 & 2\zeta_2 & \nu_2 & 0 \\ -\ell_{12} & 0 & 1 & 0 & 2(\ell_{12} - \ell_{13}) & 0 & \ell_{13} - \ell_{12} - \ell_{14} \\ 0 & -\ell_{22} & 0 & 0 & 2(\ell_{22} - \ell_{23}) & \ell_{23} - \ell_{22} - \ell_{24} & 0 \\ 0 & -\ell_{15} & 0 & \ell_{15} - \ell_{16} & 1 + \ell_{15} - \ell_{13} & 0 & \ell_{13} + \ell_{16} - \ell_{14} - \ell_{15} \\ 0 & 0 & 0 & 0 & -\ell_{13} & 1 & \ell_{13} - \ell_{14} \\ 0 & 0 & 0 & 0 & -\ell_{23} & \ell_{23} - \ell_{24} & 1 \end{pmatrix}, \quad (\text{C4})$$

where we have defined

$$\ell_{ij} = \phi(p_{i,j}), \quad (\text{C5a})$$

$$\zeta_i = \ell_{i2} + \ell_{i5} - \ell_{i1} - \ell_{i3}, \quad (\text{C5b})$$

$$\nu_i = \ell_{i1} + 2\ell_{i3} + \ell_{i6} - \ell_{i2} - \ell_{i4} - 2\ell_{i5}, \quad (\text{C5c})$$

and

$$\mathbf{b} = \begin{pmatrix} \phi(p_{1,1}) \\ \phi(p_{2,1}) \\ 0 \\ 0 \\ 0 \\ 0 \\ 0 \end{pmatrix}. \quad (\text{C6})$$

While the linear system (C3) can easily be solved nu-

merically, one can also proceed to a fully analytical solution. To this end, for a given dot index i we first express the density correlators of order higher than one in terms of the densities. This gives the smaller linear system (note that for index i the correlator $\langle \hat{n}_{i\sigma} \hat{n}_{i\bar{\sigma}} \rangle$ does not appear)

$$\mathbf{B} \begin{pmatrix} \langle \hat{n}_{i\bar{\sigma}} \hat{n}_{i\bar{\sigma}} \hat{n}_{i\bar{\sigma}} \rangle \\ \langle \hat{n}_{i\sigma} \hat{n}_{i\bar{\sigma}} \hat{n}_{i\bar{\sigma}} \rangle \\ \langle \hat{n}_{i\sigma} \hat{n}_{i\bar{\sigma}} \rangle \\ \langle \hat{n}_{i\bar{\sigma}} \hat{n}_{i\bar{\sigma}} \rangle \end{pmatrix} = \begin{pmatrix} 0 \\ 0 \\ \phi(p_{i,2}) \langle n_{i\bar{\sigma}} \rangle \\ \phi(p_{i,5}) \langle n_{i\bar{\sigma}} \rangle \end{pmatrix}, \quad (\text{C7})$$

where the matrix \mathbf{B} is given by

$$\mathbf{B} = \begin{pmatrix} 1 & 0 & \ell_{i6}(\ell_{i4} - \ell_{i6} - 1)^{-1} & 0 \\ \ell_{i3} - \ell_{i4} & 1 & 0 & -\ell_{i3} \\ 0 & 0 & 1 - \frac{\ell_{i6}(\ell_{i2} + \ell_{i4} - 2\ell_{i3})(\ell_{i4} - \ell_{i3})}{1 - \ell_{i4} + \ell_{i6}} & 2(\ell_{i2} - \ell_{i3}) + \ell_{i3}(2\ell_{i3} - \ell_{i2} - \ell_{i4}) \\ 0 & 0 & \ell_{i5} - \ell_{i6} + \frac{\ell_{i6}(\ell_{i3} + \ell_{i6} - \ell_{i4} - \ell_{i5})}{1 - \ell_{i4} + \ell_{i6}} & 1 + \ell_{i5} - \ell_{i3} \end{pmatrix}. \quad (\text{C8})$$

The solution of this smaller linear system reads

$$\langle \hat{n}_{i\bar{\sigma}} \hat{n}_{i\bar{\sigma}} \rangle = \tau_{i,1} \langle \hat{n}_{i\bar{\sigma}} \rangle, \quad (\text{C9a})$$

$$\langle \hat{n}_{i\sigma} \hat{n}_{i\bar{\sigma}} \rangle = \tau_{i,2} \langle \hat{n}_{i\bar{\sigma}} \rangle, \quad (\text{C9b})$$

$$\langle \hat{n}_{i\bar{\sigma}} \hat{n}_{i\bar{\sigma}} \hat{n}_{i\bar{\sigma}} \rangle = \tau_{i,3} \langle \hat{n}_{i\bar{\sigma}} \rangle, \quad (\text{C9c})$$

$$\langle \hat{n}_{i\sigma} \hat{n}_{i\bar{\sigma}} \hat{n}_{i\bar{\sigma}} \rangle = \tau_{i,4} \langle \hat{n}_{i\bar{\sigma}} \rangle, \quad (\text{C9d})$$

where

$$\tau_{i,1} = \frac{1}{\tau_{i,0}} [\bar{\ell}_{i2} (\ell_{i3} - 1) (\ell_{i5} - 1) + 2(1 - \ell_{i3}) \bar{\ell}_{i3} \ell_{i5} + \ell_{i3} \bar{\ell}_{i4} \ell_{i5}] , \quad (\text{C10a})$$

$$\tau_{i,2} = \frac{1}{\tau_{i,0}} \left[\bar{\ell}_{i2} \left(\ell_{i6} + \ell_{i5} \left(\frac{\ell_{i6}}{1 - \ell_{i4} + \ell_{i6}} - 1 \right) - \frac{\ell_{i6}}{1 - \ell_{i4} + \ell_{i6}} (\ell_{i3} - \ell_{i4} + \ell_{i6}) \right) \right. \\ \left. + \frac{1}{\tau_{i,0}} \left[1 - \frac{\ell_{i6}}{1 - \ell_{i4} + \ell_{i6}} (\bar{\ell}_{i2} + \bar{\ell}_{i4} - 2\bar{\ell}_{i3}) (\ell_{i4} - \ell_{i3}) \right] \ell_{i5} , \quad (\text{C10b}) \right.$$

$$\tau_{i,3} = \frac{\ell_{i6}}{1 - \ell_{i4} + \ell_{i6}} \tau_{i,1} , \quad (\text{C10c})$$

$$\tau_{i,4} = (\ell_{i4} - \ell_{i3}) \frac{\ell_{i6}}{1 - \ell_{i4} + \ell_{i6}} \tau_{i,1} + \ell_{i3} \tau_{i,2} , \quad (\text{C10d})$$

$$\tau_{i,0} = (\bar{\ell}_{i2} (\ell_{i3} - 2) + 2(1 - \ell_{i3}) \bar{\ell}_{i3} + \ell_{i3} \bar{\ell}_{i4}) \left(\ell_{i5} - \ell_{i6} + \frac{\ell_{i6}}{1 - \ell_{i4} + \ell_{i6}} (\ell_{i3} - \ell_{i4} - \ell_{i5} + \ell_{i6}) \right) \\ + \left[1 - \frac{\ell_{i6}}{1 - \ell_{i4} + \ell_{i6}} (\bar{\ell}_{i2} + \bar{\ell}_{i4} - 2\bar{\ell}_{i3}) (\ell_{i4} - \ell_{i3}) \right] (1 + \ell_{i5} - \ell_{i3}) , \quad (\text{C10e})$$

where the ℓ_{ij} are defined in Eq. (C5a). Since in this way, all the density correlators (and thus all the residues of the single-particle GF, see Eq. (23)) are expressed in terms of the densities themselves, the final step to obtain the densities requires the solution of the 2×2 linear system

$$\begin{pmatrix} \eta_{11} & \eta_{12} \\ \eta_{21} & \eta_{22} \end{pmatrix} \begin{pmatrix} \langle \hat{n}_{i\sigma} \rangle \\ \langle \hat{n}_{j\sigma} \rangle \end{pmatrix} = \begin{pmatrix} \phi(p_{1,1}) \\ \phi(p_{2,1}) \end{pmatrix} , \quad (\text{C11})$$

where the parameters $\eta_{i,j}$ are given in Eq. (25). The solution of the linear system finally gives the expression for the densities Eq. (24).

ACKNOWLEDGMENTS

We acknowledge useful discussions with Gianluca Stefanucci. We acknowledge financial support through Grant PID2020-112811GB-I00 funded by MCIN/AEI/10.13039/501100011033 as well as by grant IT1453-22 ‘‘Grupos Consolidados UPV/EHU del Gobierno Vasco’’. We acknowledge the technical support provided by SGIker (Scientific Computing Services UPV/EHU).

-
- [1] R. Hanson, L. P. Kouwenhoven, J. R. Petta, S. Tarucha, and L. M. Vandersypen, Spins in few-electron quantum dots, *Rev. Mod. Phys.* **79**, 1217 (2007).
 - [2] C. Kloeffel and D. Loss, Prospects for spin-based quantum computing in quantum dots, *Annu. Rev. Condens. Matter Phys.* **4**, 51 (2013).
 - [3] D. Loss and D. P. DiVincenzo, Quantum computation with quantum dots, *Phys. Rev. A* **57**, 120 (1998).
 - [4] P. Michler, A. Kiraz, C. Becher, W. V. Schoenfeld, P. M. Petroff, L. Zhang, E. Y. Hu, and A. Imamoglu, Quantum dots for quantum information technologies, *Science* **290**, 2282 (2000).
 - [5] J. R. Petta, A. C. Johnson, J. M. Taylor, E. A. Laird, A. Yacoby, M. D. Lukin, C. M. Marcus, M. P. Hanson, and A. C. Gossard, Coherent manipulation of coupled electron spins in semiconductor quantum dots, *Science* **309**, 2180 (2005).
 - [6] S. M. Reimann and M. Manninen, Electronic structure of quantum dots, *Rev. Mod. Phys.* **74**, 1283 (2002).
 - [7] I. Žutić, J. Fabian, and S. Das Sarma, Spintronics: Fundamentals and applications, *Rev. Mod. Phys.* **76**, 323 (2004).
 - [8] M. Veldhorst, C. H. Yang, B. Hwang, B. Huang, C. H. Yang, J. T. Muhonen, S. Simmons, A. Laucht, F. E. Hudson, R. Rahman, G. Klimeck, K. M. Itoh, A. Morello, and A. S. Dzurak, A two-qubit logic gate in silicon, *Nature* **526**, 410 (2015).
 - [9] F. A. Zwanenburg, A. S. Dzurak, A. Morello, M. Y. Simmons, L. C. Hollenberg, G. Klimeck, S. Rogge, S. N. Coppersmith, and M. A. Eriksson, Silicon quantum electronics, *Rev. Mod. Phys.* **85**, 961 (2013).
 - [10] J. R. Petta and D. C. Ralph, Studies of spin-orbit scattering in noble-metal nanoparticles using energy-level tunneling spectroscopy, *Phys. Rev. Lett.* **87**, 266801 (2001).
 - [11] F. P. Garcıa de Arquer, D. V. Dmitri V. Talapin, V. I. Klimov, Y. Arakawa, M. Bayer, and E. H. Sargent, Semiconductor quantum dots: Technological progress and future challenges, *Science* **373**, eaaz8541 (2021).
 - [12] J. Nygard, D. H. Cobden, and P. E. Lindelof, Kondo physics in carbon nanotubes, *Nature* **408**, 342 (2000).
 - [13] M. R. Buitelaar, A. Bachtold, T. Nussbaumer, M. Iqbal, and C. Schonenberger, Multiwall carbon nanotubes as quantum dots, *Phys. Rev. Lett.* **88**, 156801 (2002).
 - [14] J. J. Parks, A. R. Champagne, G. R. Hutchison, S. Flores-Torres, H. D. Abruna, and D. C. Ralph, Tuning the Kondo effect with a mechanically controllable break junction, *Phys. Rev. Lett.* **99**, 026601 (2007).

- [15] P. W. Anderson, Localized magnetic states in metals, *Phys. Rev.* **124**, 41 (1961).
- [16] A. C. Hewson, *The Kondo Problem to Heavy Fermions* (Cambridge University Press, Cambridge, 1997).
- [17] K. Ono, D. Austing, Y. Tokura, and S. Tarucha, Current rectification by pauli exclusion in a weakly coupled double quantum dot system, *Science* **297**, 1313 (2002).
- [18] W. G. van der Wiel, S. De Franceschi, J. Elzerman, T. Fujisawa, S. Tarucha, and L. Kouwenhoven, Electron transport through double quantum dots, *Rev. Mod. Phys.* **75**, 1 (2002).
- [19] J. You and H. Zheng, Electron transport through a double-quantum-dot structure with intradot and interdot coulomb interactions, *Phys. Rev. B* **60**, 13314 (1999).
- [20] Y. Zhang, S. Wang, W. Li, and M. Yue, Inverse current induced thermoelectric conversion in a parallel-coupled double quantum dot system, *Phys. Scr.* **98**, 105245 (2023).
- [21] J. Petta, A. Johnson, C. Marcus, M. Hanson, and A. Gosard, Manipulation of a single charge in a double quantum dot, *Phys. Rev. Lett.* **93**, 186802 (2004).
- [22] J. Chen, A. Chang, and M. Melloch, Transition between quantum states in a parallel-coupled double quantum dot, *Phys. Rev. Lett.* **92**, 176801 (2004).
- [23] D. Fernández-Fernández, Y. Ban, and G. Platero, Quantum control of hole spin qubits in double quantum dots, *Phys. Rev. Appl.* **18**, 054090 (2022).
- [24] D. Bouman, R. J. Van Gulik, G. Steffensen, D. Pataki, P. Boross, P. Krogstrup, J. Nygård, J. Paaske, A. Pályi, and A. Geresdi, Triplet-blockaded josephson supercurrent in double quantum dots, *Phys. Rev. B* **102**, 220505 (2020).
- [25] R. Bulla, T. A. Costi, and T. Pruschke, Numerical renormalization group method for quantum impurity systems, *Rev. Mod. Phys.* **80**, 395 (2008).
- [26] E. Gull, A. J. Millis, A. I. Lichtenstein, A. N. Rubtsov, M. Troyer, and P. Werner, Continuous-time monte carlo methods for quantum impurity models, *Rev. Mod. Phys.* **83**, 349 (2011).
- [27] H. Aoki, N. Tsuji, M. Eckstein, M. Kollar, T. Oka, and P. Werner, Nonequilibrium dynamical mean-field theory and its applications, *Rev. Mod. Phys.* **86**, 779 (2014).
- [28] U. Schollwöck, The density-matrix renormalization group in the age of matrix product states, *Ann. Phys.* **326**, 96 (2011).
- [29] P. Coleman, New approach to the mixed-valence problem, *Phys. Rev. B* **29**, 3035 (1984).
- [30] N. E. Bickers, Review of techniques in the large-n expansion for dilute magnetic alloys, *Rev. Mod. Phys.* **59**, 845 (1987).
- [31] M. Eckstein, M. Kollar, and P. Werner, Nonequilibrium dynamical mean-field theory, *Phys. Rev. Lett.* **103**, 056403 (2010).
- [32] Y. Tanimura, Stochastic liouville, langevin, fokker-planck, and master equation approaches to quantum dissipative systems, *J. Phys. Soc. Jpn.* **75**, 082001 (2006).
- [33] A. Ishizaki and G. R. Fleming, Unified treatment of quantum coherent and incoherent hopping dynamics in electronic energy transfer: Reduced hierarchy equation approach, *J. Chem. Phys.* **130**, 234111 (2009).
- [34] D. N. Zubarev, Double-time green functions in statistical physics, *Sov. Phys. Usp.* **3**, 320 (1960).
- [35] J. Hubbard, Electron correlations in narrow energy bands, *Proc. R. Soc. Lond. A* **276**, 238 (1963).
- [36] J. Hubbard, Electron correlations in narrow energy bands. ii. the degenerate band case, *Proc. R. Soc. Lond. A* **277**, 237 (1964).
- [37] J. Hubbard, Electron correlations in narrow energy bands iii. an improved solution, *Proc. R. Soc. Lond. A* **281**, 401 (1964).
- [38] Y. Meir and N. S. Wingreen, Landauer formula for the current through an interacting electron region, *Phys. Rev. Lett.* **68**, 2512 (1992).
- [39] R. Van Roermund, S.-y. Shiao, and M. Lavagna, Anderson model out of equilibrium: Decoherence effects in transport through a quantum dot, *Phys. Rev. B* **81**, 165115 (2010).
- [40] R. Świrkowicz, J. Barnaś, and M. Wilczyński, Nonequilibrium Kondo effect in quantum dots, *Phys. Rev. B* **68**, 195318 (2003).
- [41] J. You and H.-Z. Zheng, Spectral properties of a double-quantum-dot structure: A causal green's function approach, *Phys. Rev. B* **60**, 8727 (1999).
- [42] D. Sztenkiel and R. Świrkowicz, Electron transport through double quantum dot system with inter-dot coulomb interaction, *Acta Phys. Pol. A* **111**, 361 (2007).
- [43] D. M.-T. Kuo and Y.-C. Chang, Tunneling current spectroscopy of a nanostructure junction involving multiple energy levels, *Phys. Rev. Lett.* **99**, 086803 (2007).
- [44] S. Lamba and S. Joshi, Transport through a coupled quantum dot system: Role of interdot interactions, *Phys. Rev. B* **62**, 1580 (2000).
- [45] J. Palacios, L. Liu, and D. Yoshioka, Fine structure in the off-resonance conductance of small coulomb-blockade systems, *Phys. Rev. B* **55**, 15735 (1997).
- [46] M. A. Sierra, M. Saiz-Bretín, F. Domínguez-Adame, and D. Sánchez, Interactions and thermoelectric effects in a parallel-coupled double quantum dot, *Phys. Rev. B* **93**, 235452 (2016).
- [47] B. R. Bulka and T. Kostyrko, Electronic correlations in coherent transport through a two quantum dot system, *Phys. Rev. B* **70**, 205333 (2004).
- [48] Q.-F. Sun and H. Guo, Double quantum dots: Kondo resonance induced by an interdot interaction, *Phys. Rev. B* **66**, 155308 (2002).
- [49] F. Chi and S.-S. Li, Interdot interaction induced zero-bias maximum of the differential conductance in parallel double quantum dots, *J. Appl. Phys.* **99**, 043705 (2006).
- [50] Y.-C. Chang and D. M.-T. Kuo, Theory of charge transport in a quantum dot tunnel junction with multiple energy levels, *Phys. Rev. B* **77**, 245412 (2008).
- [51] Q. Feng and P. M. Oppeneer, Fast multi-orbital equation of motion impurity solver for dynamical mean field theory, *J. Phys.: Condens. Matter* **23**, 425601 (2011).
- [52] A. Hewson, Theory of localized magnetic states in metals, *Phys. Rev.* **144**, 420 (1966).
- [53] D. A. Ryndyk, R. Gutiérrez, B. Song, and G. Cuniberti, Green function techniques in the treatment of quantum transport at the molecular scale, in *Energy Transfer Dynamics in Biomaterial Systems* (Springer, Berlin, 2009) pp. 213–335.
- [54] H. Haug and A.-P. Jauho, *Quantum kinetics in transport and optics of semiconductors*, Vol. 2 (Springer, Berlin, 2008).
- [55] C. Niu, D. Lin, and T. Lin, Equation of motion for nonequilibrium green functions, *J. Phys.: Condens. Matter* **11**, 1511 (1999).

- [56] G. Stefanucci and R. Van Leeuwen, *Nonequilibrium many-body theory of quantum systems: a modern introduction* (Cambridge University Press, Cambridge, 2013).
- [57] C. W. J. Beenakker, Theory of coulomb-blockade oscillations in the conductance of a quantum dot, *Phys. Rev. B* **44**, 1646 (1991).
- [58] M. Liul, A. Ryzhov, and S. Shevchenko, Interferometry of multi-level systems: rate-equation approach for a charge qu d it, *Eur. Phys. J. Spec. Top.* **232**, 3227 (2023).
- [59] Y. Mazal, Y. Meir, and Y. Dubi, Nonmonotonic thermoelectric currents and energy harvesting in interacting double quantum dots, *Phys. Rev. B* **99**, 075433 (2019).
- [60] N. Sobrino, F. Eich, G. Stefanucci, R. D'Agosta, and S. Kurth, Thermoelectric transport within density functional theory, *Phys. Rev. B* **104**, 125115 (2021).
- [61] N. Sobrino, S. Kurth, and D. Jacob, Exchange-correlation potentials for multiorbital quantum dots subject to generic density-density interactions and hund's rule coupling, *Phys. Rev. B* **102**, 035159 (2020).
- [62] Y. Tanimura, Nonperturbative expansion method for a quantum system coupled to a harmonic-oscillator bath, *Phys. Rev. A* **41**, 6676 (1990).
- [63] Y.-A. Yan, F. Yang, Y. Liu, and J. Shao, Hierarchical approach based on stochastic decoupling to dissipative systems, *Chem. Phys. Lett.* **395**, 216 (2004).
- [64] R.-X. Xu, P. Cui, X.-Q. Li, Y. Mo, and Y. Yan, Exact quantum master equation via the calculus on path integrals, *J. Chem. Phys.* **122**, 041103 (2005).
- [65] N. Sobrino, EOM_DQD, https://github.com/Nahualcsc/EOM_DQD (2024).
- [66] G. Stefanucci and S. Kurth, Steady-state density functional theory for finite bias conductances, *Nano Lett.* **15**, 8020 (2015).
- [67] S. Kurth and G. Stefanucci, Transport through correlated systems with density functional theory, *J. Phys.: Condens. Matter* **29**, 413002 (2017).
- [68] D. Jacob and S. Kurth, Many-body spectral functions from steady state density functional theory, *Nano Lett.* **18**, 2086 (2018).
- [69] N. Sobrino, R. D'Agosta, and S. Kurth, Steady-state density functional theory for thermoelectric effects, *Phys. Rev. B* **100**, 195142 (2019).
- [70] N. Sobrino, R. D'Agosta, and S. Kurth, Thermoelectric efficiency in multiterminal quantum thermal machines from steady-state density functional theory, *Phys. Rev. B* **107**, 195116 (2023).